Impacts of the North Atlantic Subtropical High on Daily Summer Precipitation over the Conterminous United States

ENRICO ZORZETTO[a] AND LAIFANG LI[b]

[a] *Program in Atmospheric and Oceanic Sciences, Princeton University, Princeton, New Jersey*
[b] *Department of Meteorology and Atmospheric Science, Institute of Computational and Data Sciences, Earth and Environmental Systems Institute, The Pennsylvania State University, State College, Pennsylvania*

(Manuscript received 20 October 2020, in final form 1 April 2021)

ABSTRACT: By modulating the moisture flux from ocean to adjacent land, the North Atlantic subtropical high (NASH) western ridge significantly influences summer-season total precipitation over the conterminous United States (CONUS). However, its influence on the frequency and intensity of daily rainfall events over the CONUS remains unclear. Here we introduce a Bayesian statistical model to investigate the impacts of the NASH western ridge position on key statistics of daily scale summer precipitation, including the intensity of rainfall events, the probability of precipitation occurrence, and the probability of extreme values. These statistical quantities play a key role in characterizing both the impact of wet extremes (e.g., the probability of floods) and dry extremes. By applying this model to historical rain gauge records (1948–2019) covering the entire CONUS, we find that the western ridge of the NASH influences the frequency of rainfall as well as the distribution of rainfall intensities over extended areas of the CONUS. In particular, we find that the NASH ridge also modulates the frequency of extreme rainfall, especially that over part of the Southeast and Upper Midwest. Our analysis underlines the importance of including the NASH western ridge position as a predictor for key statistical rainfall properties to be used for hydrological applications. This result is especially relevant for projecting future changes in daily rainfall regimes over the CONUS based on the predicted strengthening of the NASH in a warming climate.

SIGNIFICANCE STATEMENT: The purpose of this work is studying how the position of the North Atlantic subtropical high (NASH) western ridge modulates summer daily precipitation statistics over the conterminous United States (CONUS). We introduce a Bayesian statistical model describing daily precipitation frequency, intensity, and probability of extremes. We find that the NASH is an important predictor for daily rainfall statistics over large areas of the CONUS, in particular over the Southeast and Midwest. Since the NASH is predicted to strengthen in future climate conditions, our results are particularly relevant for understanding the corresponding shift in the probability distribution and occurrence of daily precipitation.

KEYWORDS: Hydrometeorology; Bayesian methods; Statistical techniques; Probabilistic Quantitative Precipitation Forecasting (PQPF); Stochastic models; Climate variability

1. Introduction

Understanding the changing character of precipitation and flooding events in relation to both internal climate variability and anthropogenic forcing is a challenging task (Allan and Soden 2008; Westra et al. 2014; Mallakpour and Villarini 2015; Sharma et al. 2018). Data-driven analyses are often limited by the requirement of long and homogeneous rainfall records (Papalexiou and Montanari 2019) and might not be representative of future climate scenarios. On the other hand, the interannual variability in extreme precipitation frequency is linked to the internal variability of the climate system but is expected to be affected by warming conditions (Pendergrass et al. 2017). Proper characterization of these possible changes requires an adequate representation of precipitation at short aggregation time scales (e.g., at the daily to hourly time scale) in global circulation models, which remains a challenging task (Schiermeier 2010), particularly for convection and heavy precipitation events (van der Wiel et al. 2016). For these reasons, elucidating the mechanisms of precipitation's interannual variability and quantifying possible future changes in heavy rainfall regimes remains a research question of primary importance.

In hydrological studies, the adoption of nonstationary statistical models of rainfall has been widely advocated (Milly et al. 2008). However, a significant debate exists on their applications (Lins and Cohn 2011; Montanari and Koutsoyiannis 2014; Serinaldi and Kilsby 2015), since the benefit of including climate-informed covariates in the statistical analysis is often overshadowed by the additional uncertainty deriving from the adoption of complex statistical models. Therefore, in order to understand the changing character of precipitation and its connection with climate variability, it is important to develop statistical models for precipitation frequency and intensity that are able to properly exploit relevant physical information in order to reduce estimation uncertainty, while at the same time providing a robust framework for deciding whether climate variables should be included for operational purposes.

Supplemental information related to this paper is available at the Journals Online website: https://doi.org/10.1175/JHM-D-20-0242.s1.

Corresponding author: Enrico Zorzetto, ez6263@princeton.edu

DOI: 10.1175/JHM-D-20-0242.1

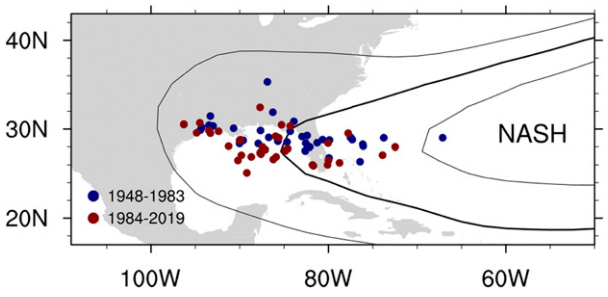

FIG. 1. Historical average summer positions of the NASH western ridge during the period 1948–2019 (colored markers) as computed from the NCEP–NCAR reanalysis. The bold curve represents the average 1948–2019 summer position of the 1560-m geopotential isoline used to define the climatological average of the ridge over the same period.

For example, such physical information can be obtained through the study of low-frequency climate variability and seasonal-averaged synoptic conditions, which are better modeled and predicted compared to short-duration rainfall accumulations. A possible way forward to resolve this issue is presented here. This work introduces a novel Bayesian statistical framework to characterize the effects of large-scale circulation on daily rainfall statistics. This approach is relevant for downscaling climate projections and predicting future changes in the probability of rainfall occurrence and intensity, including extreme events. Here we tailor this model to the conterminous United States (CONUS) and specifically use it to investigate the role of the North Atlantic subtropical high (NASH) in controlling frequency and intensity of daily summer precipitation (see appendix F for a list of acronyms used throughout the paper).

The NASH, also known as the Bermuda high, is a semipermanent high pressure system residing over the subtropical North Atlantic. It intensifies in the summer, when its western ridge extends into the CONUS, conveying moisture from ocean to land (Gamble et al. 2008; Li et al. 2011; Li and Li 2013), while also impacting the track of tropical cyclones (Kasahara 1959). In addition, from the potential vorticity view (Hoskins 1991), the advection of planetary vorticity by southerly wind along the western edge of the NASH has to be balanced by the stretching of the air column that promotes upward motion and precipitation (Wu and Liu 2003; Liu et al. 2004; Miyasaka and Nakamura 2005). As a result, precipitation preferentially occurs along the northern portion of the NASH western ridge (L. Li et al. 2012). Therefore, the spatial variations of the NASH western ridge (featured in Fig. 1 for the period 1948–2019) significantly impact atmospheric moisture fluxes and the interannual variation of total seasonal precipitation over extended regions of the United States, and especially over the Southeast (SE) (Li et al. 2011; L. Li et al. 2012; Li and Li 2013; Diem 2013).

At an interannual time scale, Diem (2006) noted that drier summers tend to occur in the SE in correspondence with a westward movement of the ridge. Furthermore, L. Li et al. (2012) found that both longitudinal and latitudinal movement of the ridge impact rainfall variation over extended areas of the CONUS. In particular, a westward movement of the ridge with respect to its climatological position increases precipitation variability, i.e., a condition in which the latitude of the ridge itself has a stronger impact on U.S. precipitation. In this case (western ridging) the meridional position of the ridge determines the sign and magnitude of the precipitation anomalies over extended regions of the CONUS: the northwest (NW) ridging deviates the moisture from the SE and the pushes the upward motion northward to the Upper Midwest, which results in dry summers over the SE, but wet conditions in the Upper Midwest and Pacific Northwest regions. Changes of the opposite sign are observed for seasonal precipitation totals in these regions in years characterized by the southwest (SW) ridging [see Fig. 4 of L. Li et al. (2012) and Fig. 8 of Li and Li (2013)]. In contrast, eastward ridging leads to reduced rainfall variability over the CONUS, so that its latitudinal position is not as relevant for seasonal rainfall.

How these seasonal-scale effects translate to the statistical properties of precipitation at the daily scale is the main research question to be addressed here. The effects of the NASH ridge on daily precipitation statistics and the frequency of heavy rainfall have been less studied than seasonal totals and are more challenging to characterize. Katz et al. (2003) introduced a family of stochastic daily weather models for temperature and precipitation which account for the NASH [therein defined as a pressure index termed Bermuda high index (BHI)] together with other climatic indices. Focusing on the winter season, they found that BHI impacts the frequency of precipitation occurrence in the SE, while significant effects on the rainfall intensity were not detected. Keim (1997) and Diem (2013) studied the correlation of the BHI with the frequency of summer heavy precipitation events over the SE. In particular, Diem (2013) found an increasing trend for rainfall variability, including in the frequency of heavy rainfall, for the Atlanta region, without finding a similar pattern in the circulation indexes examined. Recently, Nieto Ferreira and Rickenbach (2020) studied the effect of the NASH western ridge on summertime daily precipitation organization in the SE, finding that it is more relevant for mesoscale rather than for isolated precipitation features, and that NASH western ridging in the SE quadrant is associated with more precipitation along the coast and less precipitation inland, and the opposite occur in the case of NW ridging. Overall, these studies suggest that the effects of the ridge position on daily rainfall statistics are likely significant. However, a comprehensive analysis of the NASH ridge effects over the CONUS is lacking and motivates this work.

The method developed here builds on a recently developed framework to study extreme values of daily rainfall sequences (Marani and Ignaccolo 2015; Zorzetto et al. 2016; Marra et al. 2018; Miniussi et al. 2020a; Hosseini et al. 2020). Moreover, here we use a Bayesian framework for model selection in order to determine in which areas of the CONUS the adoption of climate-informed statistical models for daily precipitation is justified by historical observations, and which type of dependence structure [e.g., the dependence on both latitude and longitude of the ridge proposed by L. Li et al. (2012) as opposed to the simpler longitude dependence, or the BHI often used in past studies (Katz et al. 2003; Diem 2006)] is more

appropriate for capturing the NASH effect on daily precipitation occurrence and intensity.

Based on this Bayesian model, we investigate the connection between the position of the NASH western ridge and daily precipitation statistics over the entire CONUS, focusing on the effect on the probability distribution of rainfall intensity, probability of occurrence, and probability of extreme values. Instead of focusing on a two-value index (the BHI), here we explicitly include NASH in our statistical model by modeling continuously both the meridional and zonal positions of its western ridge, in order to capture their potentially distinct effects on daily rainfall (L. Li et al. 2012), and to evaluate where, and under which conditions, including this climate-scale feature improves the statistical representation of daily rainfall. While the model structure presented here can be generalized and applied to other climate indices, the NASH is a particularly relevant case study. Indeed, the NASH has been found to have intensified in recent years (W. Li et al. 2012): climate model simulations predict that under warming conditions the NASH will continue to intensify, with its ridge shifting westward (Li et al. 2011), and that it will be especially enhanced during spring (Song et al. 2018), thus potentially increasing the expected variability of precipitation over extended areas of the CONUS (Bishop et al. 2019a,b). Therefore, developing statistical tools to downscale climate model simulations and translate predicted shifts in the NASH climatology into impacts on finescale rainfall statistics is an increasingly important task. The statistical approach presented here serves as a step forward in the characterization of these changes, with a focus on their direct hydrological implications.

2. Data and methods

In this study we use rainfall data from the National Oceanic and Atmospheric Administration (NOAA) U.S. Historical Climatology Network (USHCN), a dataset consisting of daily rainfall records from 1218 rain gauge stations covering the entire CONUS (Menne et al. 2012b,a). This dataset is characterized by a significant fraction of station records longer than 100 years of observations, with most rain gauge records completely covering the entire study period examined here (72 years from 1948 to 2019). After retrieving the dataset, observations characterized by low quality flags were excluded from the analysis. Since our analysis is based on statistics representative of seasonal time intervals [$N_t = 92$ daily observations per year for June–August (JJA)], years characterized by more than four missing daily observations in this period were removed from the analysis. Then, only stations with at least 20 years of "complete" summer seasons in the period 1948–2019 (i.e., with less than four missing days in each season) were included in the analysis (1196 out of 1218 sites).

The seasonal average position of the NASH western ridge is here defined using the methodology proposed in L. Li et al. (2012), where the reader is referred to for additional details. Briefly, geopotential and velocity fields were obtained from the National Center of Environment Prediction–National Center of Atmospheric Research (NCEP–NCAR) reanalysis (Kalnay et al. 1996) for the period 1948–2019. The NASH ridge line was then defined as the location where the wind transitions from having an easterly to a westerly velocity component. Its intersection with the 1560-m geopotential isoline at 850 hPa (representing the NASH boundary) defines the NASH western ridge used in our analysis (Li et al. 2011). In the following analyses the seasonal JJA average position of the NASH western ridge is used, as shown in Fig. 1.

3. A Bayesian statistical model for daily rainfall frequency and magnitudes

Here we introduce the Bayesian statistical model developed for describing the daily precipitation recorded at the individual rain gauge sites. This approach models (i) seasonal rainfall totals, (ii) the seasonal number of events, (iii) the daily rainfall intensities, and (iv) the frequency of extreme daily rainfall values at each gauged site. For each of these quantities, we consider nested models of increasing complexity obtained by including or not the effect of the latitudinal and longitudinal variability of the NASH western ridge. For each variable and each location, we then select the best model by means of an information criterion described below, and based on these results we then characterize the spatial distribution of the NASH ridge impacts on daily precipitation over the CONUS domain.

a. Notation

Let n_j be the number of events observed over a season, defined here as the number of days with a 24-h rainfall accumulation recorded in excess of a threshold set to $q = 1$ mm day^{-1}. This low threshold allows us to exclude from the analysis days characterized by trace precipitation amounts that are not relevant for our analysis, while allowing the statistical model to better capture most of the distribution of daily rainfall intensities. In our case the summer season is defined as the three months JJA, with a total number of 92 daily observations per year (thus $N_t = 92$ is the seasonal number of rainfall accumulations recorded in each year j), with $j = 1, \ldots, J$, where J is the number of years in a station record. We denote with h_{ij} the magnitude of the ith daily rainfall event in excess over q within the jth time period with $i = 1, \ldots, n_j$. For each season, we are also interested in investigating the distribution of the seasonal total precipitation S_j and the seasonal maximum rainfall accumulation $h_j^{(m)}$. We include as possible model covariates the zonal and meridional positions of the NASH ridge. Specifically, along latitudinal and longitudinal coordinates we standardize the summer average ridge position in year j around its JJA climatological mean

$$y_{nj} = \frac{y_{\mathrm{LAT},j} - \mu_{\mathrm{LAT}}}{\sigma_{\mathrm{LAT}}}, \quad x_{nj} = \frac{x_{\mathrm{LON},j} - \mu_{\mathrm{LON}}}{\sigma_{\mathrm{LON}}}, \tag{1}$$

where μ_{LAT}, σ_{LAT} and μ_{LON}, σ_{LON} are means and standard deviations, respectively, of the position of the ridge in the zonal and meridional directions ($x_{\mathrm{LON},j}$ and $y_{\mathrm{LAT},j}$, respectively) represented in Fig. 1 for the 1948–2019 period.

b. Models for the dependence on the ridge position

Our objective is to model the dependence on the NASH ridge location (normalized longitude x_{nj} and latitude y_{nj}) of a

set of parameters encoding the key statistical properties of the local rainfall regimes. For each of these parameters, we test four types of dependence encompassing the possible effects of the NASH ridge position postulated in previous studies. First, we consider a model in which the ridge position does not impact rainfall intensity or frequency [No Dependence model (NOD)]. Second, we consider a simple dependence on the NASH ridge longitude [Longitude Dependence model (LOND)], consistent with previous studies based on the BHI, which measures the strength of the pressure difference between Bermuda and New Orleans (e.g., Katz et al. 2003). Conversely, the Latitude Dependence model (LATD), represents the case of rainfall anomalies responding uniquely to the latitude of the ridge. Finally, we consider a more complex Longitude-Weighted Latitudinal Dependence model (LWLD), which describes a dependence of the type found by Li et al. (2011) for seasonal totals. In this formulation rainfall anomalies still depend uniquely on the latitude of the ridge, but the strength of this effect is modulated by the ridge longitudinal position. Testing these different models over the entire CONUS will elucidate the existence of possibly spatially variable mechanisms of NASH dependence for daily scale rainfall. However, the different complexity (e.g., different number of parameters) of these different types of ridge dependence must be accounted for when selecting the best model for a given location, as will be described in section 3f. The mathematical formulation of these dependence structures is reported in appendix A.

c. Model for the seasonal number of events

We consider two models describing the probability of observing n_j rainfall events during one summer: A simple binomial model, and a Markov chain (MC) model. In the first case, the occurrence of daily rainfall is completely described by a single parameter representing the frequency of arrival of rainfall events. While the binomial distribution is the most parsimonious model, its adoption implies serial independence in the sequence of wet–dry states which may not be justified in general. Therefore, to test whether the NASH ridge position also impacts the serial dependence properties of daily rainfall occurrence, we consider a MC model to describe the occurrence of daily rainfall events, as often done in daily weather generator models (Katz and Zheng 1999; Katz et al. 2003). This model can be used to estimate the possible effect of the NASH ridge position not only on the seasonal number of events n_j, but also on the persistence of wet and dry spells, which is captured by a second parameter. For both models, the parameters describing rainfall rate of arrival and day-to-day memory are allowed to depend on the ridge position through any of the four dependence models introduced in section 3b. For a complete description of the two models for n_j, see appendix B.

d. Model for the daily event rainfall magnitudes

Several distributions have been proposed to model daily rainfall accumulations and in particular its right tail (Papalexiou et al. 2013). These include the gamma (Stechmann and Neelin 2014), stretched exponential, or mixture of normals distributions (Li and Li 2013). Here we choose a stretched exponential or Weibull distribution as this model (i) can be connected to the physics of convective rainfall events (Wilson and Toumi 2005) and (ii) it has been widely used and tested over the CONUS (Marani and Ignaccolo 2015; Zorzetto et al. 2016; Papalexiou et al. 2018; Marra et al. 2018), including in applications to remotely sensed rainfall datasets (Zorzetto and Marani 2019, 2020). Moreover, the argument by Wilson and Toumi (2005) offers some insight on the expected value of its shape parameter controlling the tail decay for convective rainfall, indicating a subexponential behavior (i.e., a distribution characterized by a ''fatter tail'' when compared to an exponential decay), but still retaining a characteristic scale. This information is helpful in characterizing the frequency of extremes from samples of limited length (Zorzetto et al. 2016). The Weibull distribution has two parameters which control its shape and scale (i.e., characteristic intensity of the events), respectively. In our analysis, we assume a constant value for the shape parameter, while allowing the (logarithm of the) scale to vary year-to-year based on the position of the ridge as described in section 3b. See appendix C for the complete model formulation for rainfall intensity.

e. Posterior computation

Given the structure of the models above, the posterior probability distribution of the quantities of interest is not available analytically. Therefore, we approximate numerically the posterior distribution using the Hamiltonian Monte Carlo technique using the Stan language (Carpenter et al. 2017). For each model and each site, we run four parallel Markov chain Monte Carlo (MCMC) chains with 2000 iterations for each chain, and discard the first half for each chain to account for the burn-in period. Therefore, we obtain $S = 4000$ samples for the posterior for each model parameters, which are used to compute posterior predictive distribution of the quantities needed to characterize the rainfall regime at each site and its dependence on the ridge position.

f. Evaluation of predictive accuracy

For the purpose of this study we need to compare several models of increasing complexity in order to evaluate whether or not climatic information should be included in probabilistic models of daily precipitation. In particular, for each study site and rainfall variable we want to learn which of the proposed dependence models is supported by the observations. Therefore, the varying complexity of the different models must be accounted for when evaluating their respective performance. After fitting the models to the station data following the procedure outlined in section 3e, we evaluate the likelihood of observing the data (e.g., the seasonal number of events n_j or their intensities x_{ij}) given the model parameters estimated through the MCMC simulations. To correct for the tendency of models of different complexity of overfitting the training data, we employ the logarithm of the pseudomarginal likelihood (lpml), described in appendix E. This measure of predictive accuracy provides an approximation to the model likelihood for a leave-one-out observation (Gelfand and Dey 1994). This model validation is performed independently for all the variables of interest (rainfall frequency, intensity, seasonal totals). For each station site and rainfall variable, the model with the

largest lpml is selected as the best description of the local daily rainfall distribution. Therefore, the spatial distribution of the "best models" over the CONUS domain characterizes the effects of the ridge position.

g. Extreme value statistics

Once we have defined models for daily rainfall events occurrence and magnitudes, we can use them to estimate the probability of extreme events. Here we focus our attention on the LWLD model, using Eq. (B1) for the probability of event occurrence, and Eq. (C1) to model daily event magnitudes, which we assume independent and identically distributed conditional to their occurrence. In this case using the Markov Chain model for n_j would not produce significant differences in the statistics of extremes, so we use the simplest binomial model for n_j. To test to what extent the frequency of extremes is impacted by NASH ridge position, we adopt the following strategy: (i) we fit the LWLD models for both event occurrences and magnitudes to the historical data at each site; (ii) we generate 100 years of synthetic data from the model specification (posterior predictive distribution); Then (iii) we extract the annual maxima values corresponding to two contrasting scenarios: The NASH western ridge located in the NW quadrant (i.e., $y_N = 1$, $x_N = -1$) and the NASH western ridge located in the SW quadrant (i.e., $y_N = -1$, $x_N = -1$). For both scenarios, the 100 generated summer maxima daily values are extracted for each of the 4000 draws from the posterior distribution. Mean values and standard deviations are then computed over the 4000 MCMC samples. As customary in extreme value analysis, we compute the rainfall quantiles corresponding to different values of return time T_r, which measures the average recurrence intervals (in years) of an event characterized by a given rainfall accumulation magnitude. Then, for a given return time value, we compute the normalized differences in estimated quantiles $\Delta q_{T_r} = [q_{\mathrm{NW}}(T_r) - q_{\mathrm{SW}}(T_r)]$. To estimate the effect size of these differences, we normalize them by either the standard deviation of the 4000 MCMC replicates for the same return-time value ($\sigma_{q_{\mathrm{SW}}(T_r)}$) or by its expected value $q_{\mathrm{SW}}(T_r)$. This procedure allows us to quantify how, based on the LWLD model, a shift in the NASH ridge position from the SW to the NW quadrant would impact the distribution of extreme rainfall across the CONUS. To further test the robustness of this procedure, we implement an independent model for the frequency of extreme values. We employ the binomial model introduced in Eq. (B1) to model the frequency of peaks over high thresholds (selected so as to have an average of two and four excesses per year during JJA, respectively) and compare the four models (NOD, LOND, LATD, and LWLD). This analysis does not determine how significant the effect of NASH ridge position is, but rather provides a measure of the potential effect size. A rigorous procedure for model selection is discussed next.

4. Results

a. Results for selected stations

We start by discussing an application of the model to the station located in Chapel Hill (North Carolina), in the southeast Atlantic region, area where the effects of NASH have been traditionally studied (Katz et al. 2003; Li and Li 2013). To test whether the model for rainfall frequency n_j and intensity h_{ij} provides a good fit to the data, we compare the samples observed for the Chapel Hill station with synthetic data generated after fitting the model, for the same historical positions of the NASH ridge (Figs. 2a–f). These posterior predictive checks show that overall the rainfall frequency and intensity are well described by the model. Figure 2g shows that the dependence of n_j on the latitudinal ridge position appears coherently captured by the model, with northward NASH ridge anomalies determining a shift of n_j toward lower values, i.e., toward drier conditions. The model also provides a good description of the frequency of extreme rainfall for this site, which is quantified by the daily rainfall magnitudes corresponding to different values of return time. This is shown in Fig. 2h, which compares historical observations and model-simulated values based on the historical NASH ridge positions. If instead we consider model predictions obtained by moving the ridge one standard deviation northwest or southwest of its climatological average, we find that for Chapel Hill the distribution of extreme rainfall remains virtually unchanged (Fig. 2i). Therefore, for this site the ridge position modulates rainfall frequency but does not significantly impact the distribution of extreme daily rainfall.

This is not the case for other sites. For example, changes in both rainfall frequency and extreme value statistics can be observed for sample sites located in Mississippi (Figs. 3a–c), Wisconsin (Figs. 3d–f), and Tennessee (Figs. 3g–i), regions characterized by a strong dependence on the ridge location.

In the case of the Mississippi site, the dependence of the number of events is similar to that of Chapel Hill, but in this case an effect on extremes also appears, with a southwestern position of the ridge leading to a shift in the distribution of extreme rainfall toward larger values (Fig. 3c). A qualitatively similar—albeit weaker in size—behavior is observed for the Tennessee station (Fig. 3i). The Wisconsin site shows the opposite behavior, with a northwest ridge position corresponding to an increase in extreme rainfall frequency when compared to a southwestern ridge position (Fig. 3f). In this case the n_j ridge dependence appears weaker when compared to the other sites (as also observed in Fig. 4b), and therefore the NASH-induced shift in the distribution of seasonal maximum rainfall is primarily driven by changes in the distribution of daily rainfall intensities h_{ij}. These results for selected stations are useful for assessing the ability of the model in reproducing the distribution of daily rainfall as well as for quantifying changes in rainfall frequency and extreme value quantiles driven by anomalies in the ridge position. We now extend the analysis to the entire CONUS so as to investigate the spatial variability of these effects.

b. Rainfall frequency and intensity distributions

To gain insights on the effects of NASH ridge position on U.S. summer precipitation over the entire CONUS, we start by reporting its effect on seasonal total rainfall in JJA, although this quantity has been the object of previous investigations (e.g., Li et al. 2011). This analysis is made possible by means of a model similar to that developed for daily precipitation (described in appendix D), in which again the variability of a

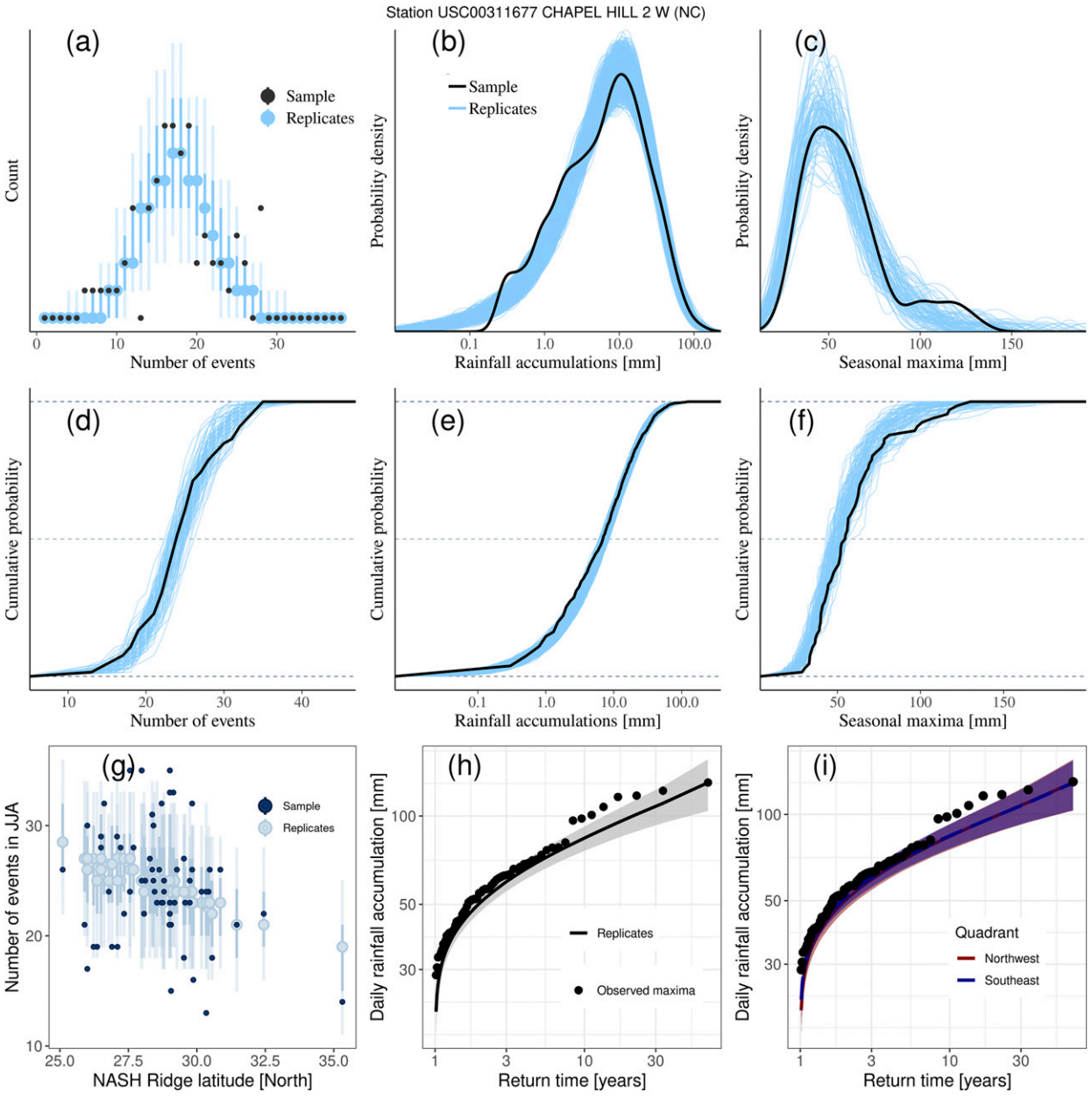

FIG. 2. Posterior predictive checks for the Chapel Hill (NC) station. (top) Observed samples with 100 MCMC replicates for (a) the number of events n_j, (b) all daily rainfall values h_{ij}, and (c) seasonal maxima values $h_j^{(m)}$ (kernel density estimation is used to represent the pdfs of h_{ij} and $h_j^{(m)}$, while the histogram of n_j is accompanied by mean and 0.9 probability bands of the MCMC samples). (d)–(f) The corresponding cumulative distribution functions are reported. (g) The n_j sample and MCMC draws (mean and 0.9 probability bands) as a function of the NASH ridge latitude. (h) Comparison of the observed annual maxima sample $h_j^{(m)}$ with the corresponding MCMC draws obtained from the observed NASH ridge positions (black line represents the mean, and the shaded area the 1σ intervals) as a function of the return time. (i) Similarly, a comparison of the same annual maxima sample with MCMC replicates obtained under the scenario of a ridge permanently in its NW position ($y_n = 1, x_n = -1$, red line and 1σ bands) and SW position ($y_n = -1, x_n = -1$, blue line and 1σ bands).

stretched exponential scale parameter describes the effect of NASH ridge on the characteristic magnitude of seasonal total rainfall.

Seasonal rainfall totals exhibit dependence on the NASH ridge position over extended areas of the CONUS, as expected from previous studies (Figs. 4a,b). The dependence on the NASH ridge longitude appears strongest in the Upper Midwest, where an eastward shift of the ridge determines a coherent regional decrease in the expected total summer rainfall. An effect of the opposite sign is observed in other parts of the country, e.g., along the East Coast, although it appears weaker and less spatially coherent. Notably, this is the case for

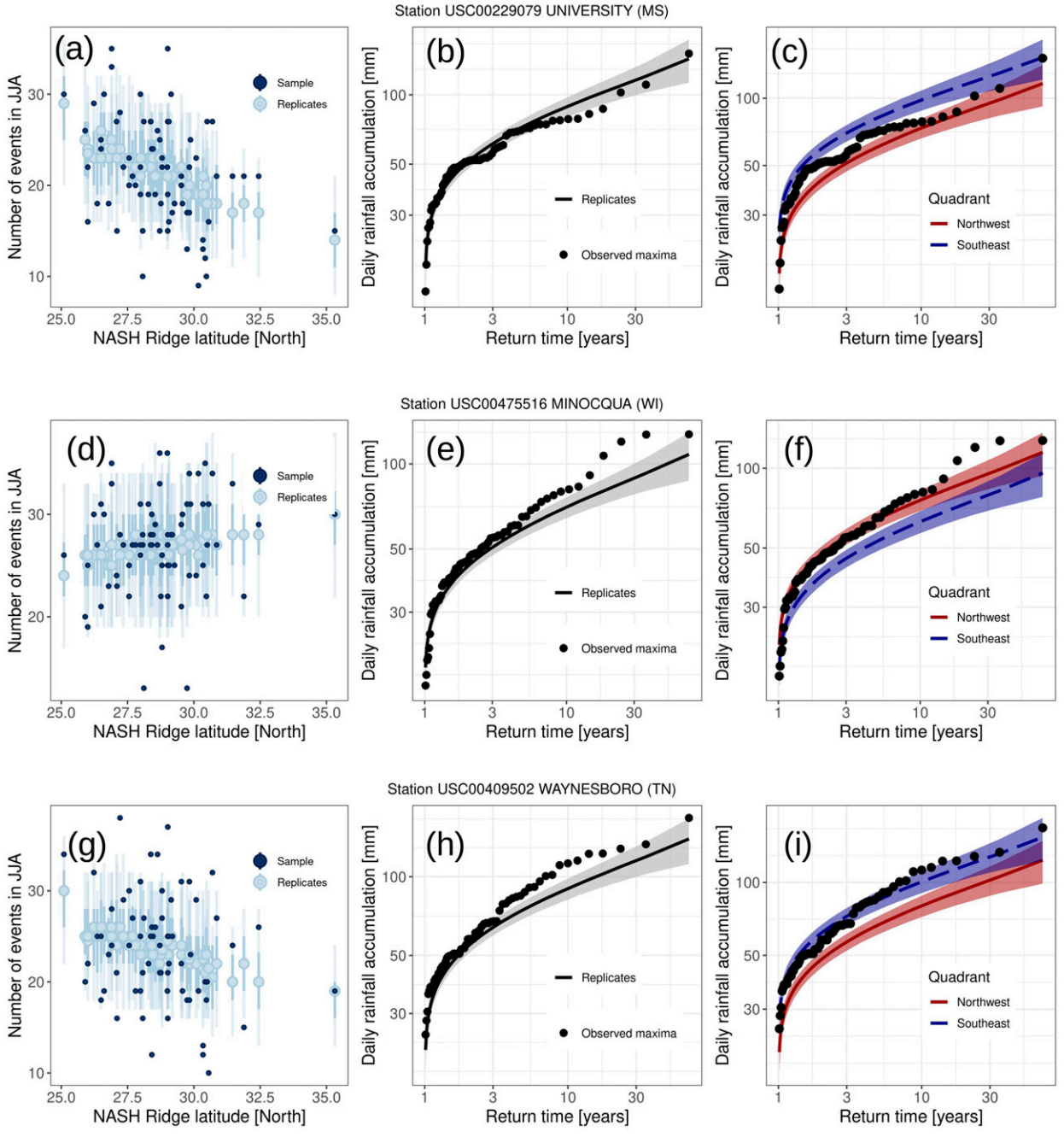

FIG. 3. As in Figs. 2g–i, but for three sample sites.

most of the SE, where the LOND is seldom selected as the best dependence model (Fig. 4a). On the other hand, LWLD is consistently selected as the best model throughout the SE, where a northwestern shift in position of the ridge is associated with a drier summer (Fig. 4b). Under the same NASH conditions, effects of the opposite sign are observed in the Pacific Northwest and in the upper Michigan, Wisconsin, and Minnesota region, characterized by a dependence on the NASH ridge latitude (LATD or LWLD models), with a wetter summer associated to north or northwest shift of the ridge, respectively. In most of the West and particularly the Southwest the effects of the ridge position appear weak or nonexistent, so that the best model selected most frequently is NOD, suggesting no relevant benefit in introducing any dependence on the ridge position in seasonal total rainfall models.

The seasonal number of events exhibits an overall dependence on the ridge position, which is qualitatively similar to

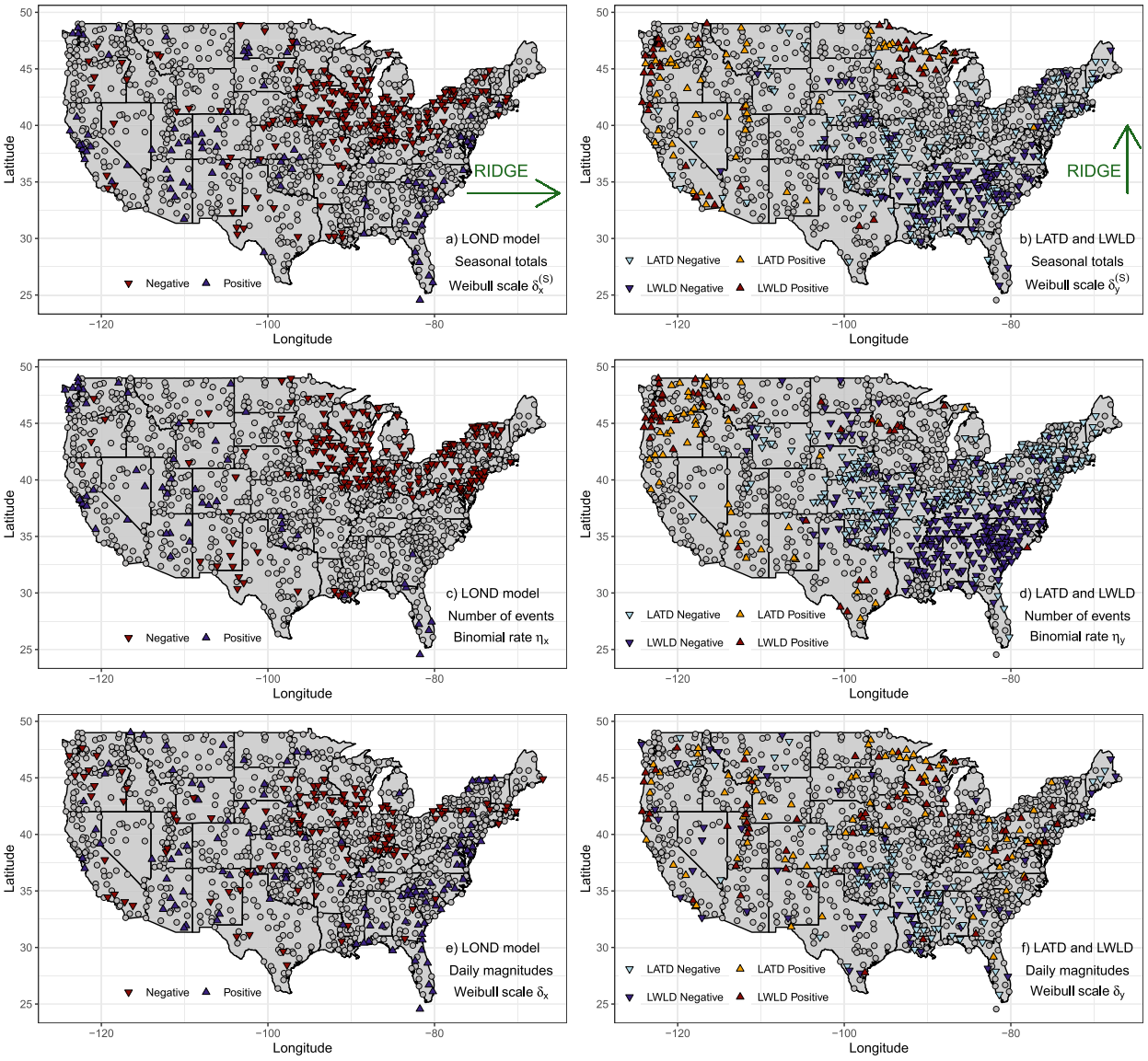

FIG. 4. Effects of the NASH ridge position on the model parameters describing (a),(b) seasonal rainfall totals; (c),(d) the seasonal number of events; and (e),(f) the daily rainfall characteristic intensity. (left) Stations where LOND is selected as the best dependence model and (right) stations where LATD or LWLD are the best model. Stations for which the model considered does not have the best performance (as quantified by the lpml) are reported in the background as gray circles. The sign of the triangle markers indicates the effect of a shift of the NASH ridge on the relevant model parameter. Upward triangles indicate that a shift in the NASH ridge position (an eastward shift in the case of the LOND model, or a northward shift in the case of the LATD/LWLD models) would determine an increase in the parameter value, i.e., wetter conditions [(a) and (b)], more frequent events [(c) and (d)], or more intense events [(e) and (f)], while the opposite is the case for stations marked by downward triangles.

that observed for seasonal rainfall totals. However, in the case of n_j the effect of NASH ridge appears stronger, more extended, and more coherent in space. Again, a longitude-only dependence on the NASH ridge position characterizes the Upper Midwest and part of the Northeast, with an eastward shift of the ridge determining a decrease in the frequency of daily rainfall events over the entire region (Fig. 4c).

Over the SE, LWLD is systematically selected as the best model, with northward NASH ridge anomalies being associated to a decrease in the seasonal frequency of rainfall throughout the SE (Fig. 4d). This finding is consistent with the NASH primarily affecting the seasonal average advection of atmospheric moisture to the region, without significantly changing the mechanisms generating precipitation events at the daily scale. The effect of NASH ridging on daily rainfall frequency appears still relevant in the Lower Midwest (with a northward anomaly again shifting the distribution of n_j toward lower values). However, in this region the dependence on the zonal

position of the ridge does not seem to impact rainfall statistics as it does in the SE, and the best model selected for most of this region is LATD rather than LWLD. Conversely, the same conditions of northward shift in the NASH ridge determine a consistent increase in the precipitation occurrence rates over the Pacific Northwest, where for a significant number of stations the best models are again LWLD and LATD, closer to the coast and inland, respectively.

However, the wetter conditions found for seasonal totals in the upper Michigan, Wisconsin, and Minnesota for a northward shift of the NASH ridge do not appear to be as significant in the case of n_j, suggesting that instead they may originate from a shift in the distribution of daily rainfall accumulations toward larger values rather than from an increase in the seasonal number of events. Conversely, the NASH effect observed for the distribution of n_j over the Pacific Northwest is spatially coherent with that found for seasonal totals. Again, in most of the western United States—except the Pacific Northwest—there is little spatially coherent dependence on the ridge position, and the model with no dependence is generally selected as having the best performance.

The effect of NASH ridge on the characteristic intensity of daily rainfall [as represented by the x_{nj} and y_{nj} dependence term of Weibull scale parameter, δ_y in Eq. (C1)] appears more limited and less coherent in space over most of the CONUS (Figs. 4e,f) when compared to the effects observed for seasonal totals and for the rainfall frequency of occurrence. However, some localized effects of the NASH ridge position are nevertheless observed. Analyzing the dependence on the latitudinal position of the ridge (LATD and LWLD models, Fig. 4f) reveals that an increased rainfall intensity over the upper Michigan, Wisconsin, and Minnesota and a decrease in parts of the South (Louisiana, Mississippi) are associated with northward NASH ridge anomalies. The consistent effect observed over upper Michigan, Wisconsin, and Minnesota confirms the hypothesis that over this region changes in seasonal totals are primarily driven by the NASH ridge position modulating the intensity distribution of rainfall events rather than their frequency of occurrence. The opposite occurs over the Pacific Northwest region, where the ridge position is associated with changes in rainfall frequency rather than in the distribution of intensities. Moreover, a longitudinal dependence in the Upper Midwest can be observed also in the case of daily rainfall intensities, although it appears less spatially extended when compared to the result obtained for rainfall frequency. Therefore, in this case the effect of NASH on rainfall totals appears to be primarily driven by changes in rainfall frequency for most stations in the Upper Midwest (Fig. 4e).

To further characterize the effect of the NASH ridge position on rainfall occurrence, we also test the Markov chain model [Eq. (B4)], which describes not only the seasonal frequency of daily rainfall events, but also the possible persistence of wet and dry states. For the seasonal number of events (Figs. 5a,b), the result appears consistent with that obtained for the simpler binomial model. The variation of the serial correlation of precipitation at 1-day temporal lag, on the other hand, appears less spatially coherent, especially in the case of longitudinal dependence on the ridge position (Fig. 5c). However, local spatially coherent effects of the NASH ridge latitude on the persistence of wet and dry states can be observed for the coastal Pacific Northwest region and for part of the Midwest (Fig. 5d). Over these regions, a northward shift in the NASH ridge position leads to increased temporal correlation of the daily rainfall occurrence. The opposite effect is observed for part of the SE. However, the sign of these changes is contrasting over most of the CONUS, so that overall the potential effects of NASH ridge on the persistence of wet and dry states are not as robust as those observed in the case of the seasonal number of events.

c. NASH ridge effects on extreme rainfall

We now turn our attention to the probability of extreme rainfall, examining the differences Δq_{T_r} between the distributions of seasonal maxima values generated in the case of a stationary ridge in the NW and SW quadrants, respectively, under the LWLD ridge dependence model. Figure 6 shows Δq_{T_r} normalized by the standard deviation of the MCMC estimates for the same quantiles ($\sigma_{q_{T_r}}$, Fig. 6a) and by their expected values q_{T_r} (Fig. 6b). These quantities correspond to the difference between the two extreme value estimates corresponding to different ridge positions (e.g., those reported in Fig. 3c, normalized either by the width of their credibility intervals $\sigma_{q_{T_r}}$ or by their expected value q_{T_r}).

For most of the stations over the CONUS, the effect of the ridge on the distribution on extremes appears limited in size. However, in several areas the dependence can be relevant. A northward ridge anomaly determines a decreased probability of extremes in part of the Southeast, although the effect seems more relevant for inland sites when compared with coastal regions. A possible explanation for this behavior is that coastal regions are more affected by tropical systems (Kunkel et al. 2013), potentially lowering their dependence on the NASH ridge position. An increased probability of extremes is observed primarily at sites located in the Pacific Northwest or in the Great Lakes region, where we also observed that the distribution of daily rainfall values is impacted by the ridge position. Note that this result for extreme rainfall depends on the assumptions on the model used, with dependence on both x_{nj} and y_{nj}. Namely, daily rainfall occurrence follows a binomial distribution, and the intensities of daily events are independent and distributed according to Eq. (C1). To independently test the robustness of our results to these modeling assumptions, we additionally examine the frequency of excesses over a high threshold, fixed by imposing the condition that for each time series, on average only four events exceed the threshold in each season. The result of this analysis confirms the extreme precipitation anomalies predicted over the SE, Upper Midwest, and Pacific Northwest (Fig. 7a). While the spatial distribution of these anomalies is consistent with that predicted by the Weibull model (Fig. 6b), the NASH ridge dependence in the case of heavy rainfall appears less spatially extended when compared to the effects observed for n_j and seasonal totals S_j. The LOND model again predicts a decrease in heavy rainfall events in the Upper Midwest (Fig. 7b), which is expected given the similar effects observed for both precipitation frequency (Fig. 4c) and intensity (Fig. 4e).

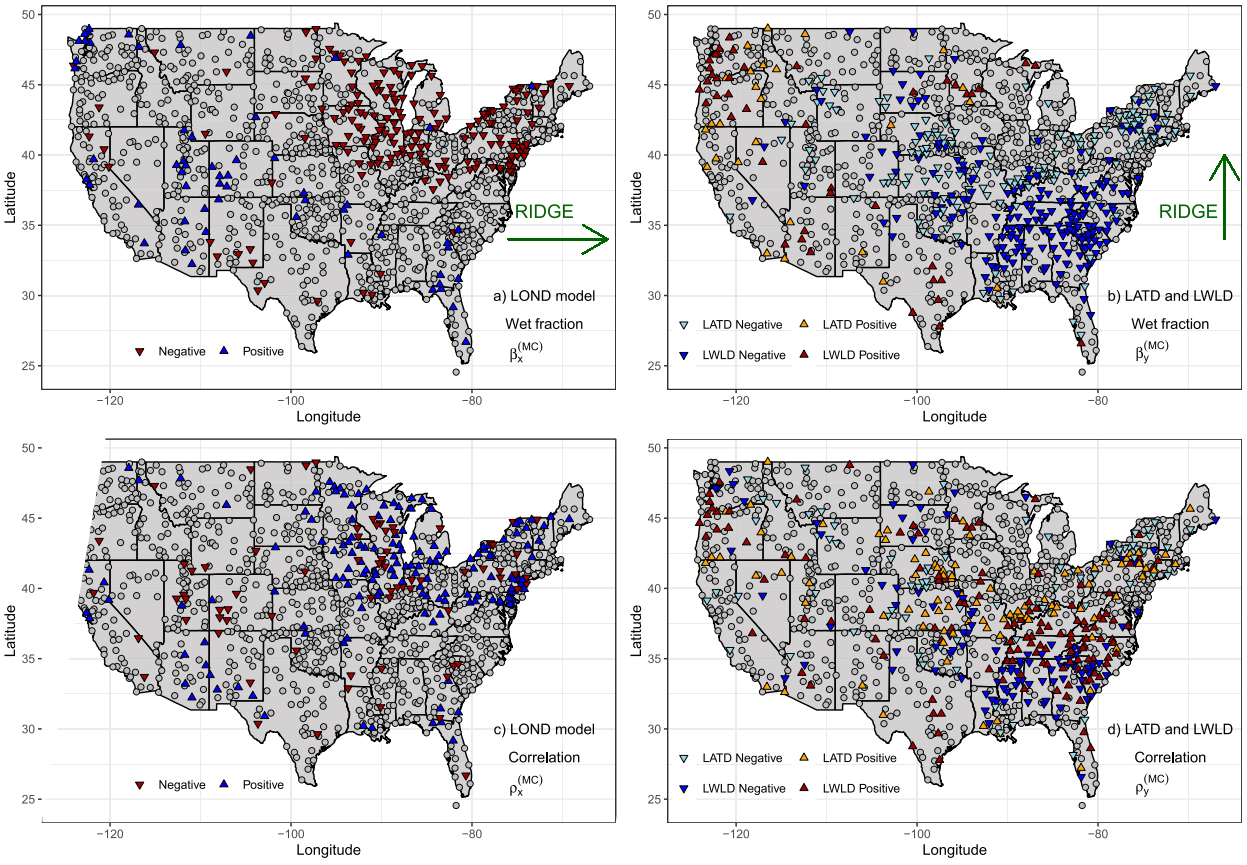

FIG. 5. Effects of the NASH ridge position on the Markov chain model parameters describing the (a),(b) frequency of occurrence of daily events, and (c),(d) the 1-day temporal autocorrelation of the wet–dry sequence. (left) Stations where LOND is selected as the best dependence model, and (right) stations where LATD or LWLD are the best model. Stations for which the model considered does not have the best performance (as quantified by the lpml) are reported in the background as gray circles. The sign of the triangle markers indicates the effect of a shift of the NASH ridge on the relevant model parameter. Upward triangles indicate that a shift in the NASH ridge position (an eastward shift in the case of the LOND model, or a northward shift in the case of the LATD/LWLD models) would determine an increase in the parameter value, i.e., more frequent events [(a) and (b)] of increased correlation of the wet–dry sequence [(c) and (d)], while the opposite is the case for stations marked by downward triangles.

This analysis confirms the association of increased probability of intense daily rainfall over the Pacific Northwest with a northward shift of the ridge, and a decrease over the SE under the same conditions. The longitude dependence also in this case appears relevant only over the Upper Midwest, where an eastward movement of the NASH ridge leads to decreased probability of threshold exceedance.

5. Discussion

We found that the NASH ridge primarily impacts the frequency of summer rainfall over extended areas of the United States, and to a smaller extent also modulates the intensity of events at the daily scale. In large areas of the country, the lpml-based framework for model selection suggests that including zonal and meridional components of the ridge position is supported by the data, even after accounting for the increased model complexity. Over extended areas of the CONUS (primarily over the Southeast; upper Michigan, Wisconsin, and Minnesota; and Pacific Northwest regions) the latitude of the NASH western ridge significantly modulates the statistical properties of daily rainfall. A notable exception is part of the Midwest, where the longitudinal position of the ridge appears more appropriate to explain the interannual variability of summer precipitation. A qualitative summary of these effects is reported in Table 1. The dependence detected for the distribution of event intensities is much weaker than that observed for seasonal total rainfall and event occurrences, and the stations for which this dependence is relevant are sparser.

Overall, the impacts of the ridge appear much weaker over most of the West. A noteworthy exception is our finding that the impacts on precipitation daily statistics extend to the Pacific Northwest, where the moisture flux from the Atlantic Ocean can hardly reach. These counterintuitive results can be understood by taking into account the remote factors that impact the NASH western ridge movement. Studies have shown that the SW ridging involves air–sea interaction over the Gulf of Mexico (Hu et al. 2011; L. Li et al. 2012; Ryu and Hayhoe 2014), while the

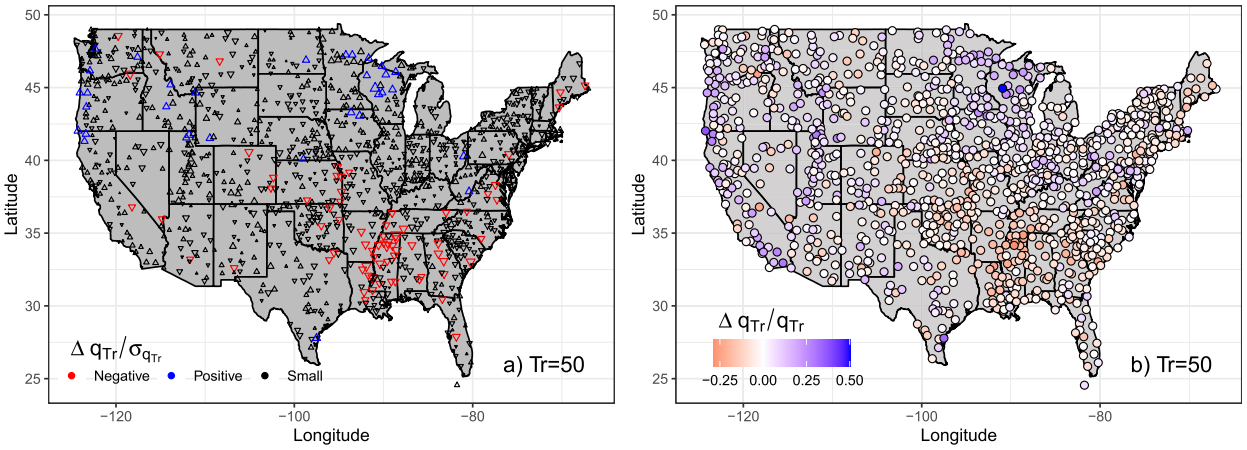

FIG. 6. Effect of the ridge position on extreme summer rainfall statistics. Differences Δq_{T_r} between expected extreme rainfall quantiles computed for NASH ridge permanently in the NW quadrant ($y_n = 1, x_n = -1$) with respect the same quantiles computed for NASH ridge permanently in the SW quadrant ($y_n = -1, x_n = -1$). For each site, Δq_{T_r} was normalized (a) by the standard deviation $\sigma_{q_{Tr}}$ of the 4000 MCMC replicate samples or (b) by their expected values q_{T_r}. Results are reported for a 50-yr return time. Upward red triangles correspond to locations where a NW ridge determines an increased probability of extremes larger than one $\sigma_{q_{T_r}}$, while downward blue triangles correspond to locations where a NW ridge determines a decrease in the probability of extremes of at least $\sigma_{q_{T_r}}$. Sites with variations of smaller magnitude are reported in black, again with the direction of the triangle representing the sign of the change. The sign of the triangle is proportional to the magnitude of $\Delta q_{T_r}/\sigma_{q_{T_r}}$.

NW ridge shows association with Pacific decadal oscillation (PDO; L. Li et al. 2012). With a positive phase of PDO, the warm SSTA over the northeastern Pacific excited a barotropic wave train emanating from the northwestern coast of the United States, propagating downstream and converging over the SE. The wave train is featured by a low pressure over the Pacific Northwest and a high pressure over the SE, and thus leads to opposite precipitation anomalies over the two regions. Thus, the observed precipitation anomalies over the Pacific Northwest are not to be interpreted as a direct result of NW ridging, but rather of the wave train pattern that leads to NW ridging.

Our results are in agreement with previous studies focusing on summer precipitation totals (L. Li et al. 2012) and show how frequency and characteristic intensity of daily rainfall contribute to the observed precipitation anomalies over a season.

The results of this analysis underline the importance of including the position of the NASH ridge in stochastic modeling of daily precipitation over the CONUS. This is especially

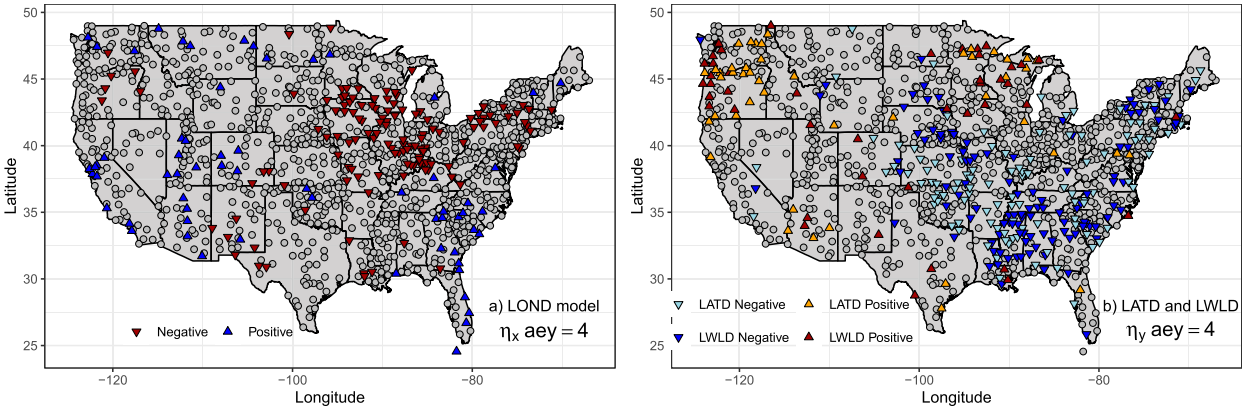

FIG. 7. Effects of the NASH ridge position on the frequency of rainfall events exceeding high thresholds, selected so that on average 4 events per year exceed the threshold during JJA. (a) Stations where LOND is selected as the best dependence model; (b) stations where LATD or LWLD are the best model. Stations for which the model considered does not have the best performance (as quantified by the lpml) are reported in the background as gray circles. The sign of the triangle markers indicates the effect of a shift of the NASH ridge on the relevant model parameter. Upward triangles indicate that a shift in the NASH ridge position (an eastward shift in the case of the LOND model, or a northward shift in the case of the LATD/LWLD models) would determine an increase in the frequency of threshold exceedance for a given JJA season, while the opposite is the case for stations marked by downward triangles.

TABLE 1. Summary of the best models over representative regions of the CONUS for rainfall intensity, frequency of occurrence, and seasonal totals.

Region	Intensity (h_{ij})	Frequency (n_j)	Totals (S_j)
Southeast	NOD/LWLD/LATD	LATD/LWLD	LATD/LWLD
Upper Wisconsin and Minnesota	LWLD/LATD	NOD	LWLD/LATD
Central and Upper Midwest, part of Northeast	NOD/LOND	LOND	LOND
Pacific Northwest	NOD	LATD/LWLD	LATD/LWLD
West	NOD	NOD	NOD

relevant for hydrological applications and for predicting daily scale rainfall variability in future climate conditions. Notably, given the strengthening of the NASH predicted under warming climate conditions (W. Li et al. 2012), accounting for its effects on rainfall variability will become increasingly important. The statistical framework proposed here and its application to historical records over the CONUS suggest the opportunity of adopting such an approach to learn the relation between the NASH and daily rainfall statistics, and in turn use this information to downscale climate model outputs to characterize the statistical properties of daily rainfall under future climate conditions.

Modeling seasonal extreme values by assuming event independence and a Weibull distribution of daily accumulations, we show that the effects of the NASH ridge position on frequency and intensity of events also affect the distribution of extreme rainfall. To further test this result, we run a similar analysis modeling the frequency of the largest peaks over threshold for each time series, and we find that the spatial distribution of rainfall anomalies is consistent with the Weibull model. In particular, northwestern ridging is connected with a decreased probability of extreme summer rainfall over the Southeast and parts of the Midwest, while an effect of opposite sign—although weaker and lesser in extent—is observed in the Upper Midwest (western Great Lakes region, primarily Minnesota and Wisconsin). In this region the NASH ridge position affects the intensity more than the frequency of daily rainfall events.

It is noteworthy that the analyses here have been performed independently for each observed time series and thus should be interpreted as representative of the rainfall field at a point in space. As a consequence, the regional effects listed in Table 1 remain qualitative. To extend our results over extended regions, a spatial version of the model proposed here should be specified. A simple example of this extension is the "*borrowing strength*" approach (Katz et al. 2003), which consists in pulling together observations by nearby stations assuming that they exhibit a similar response to NASH ridge anomalies. This method can be applied over a region of interest to determine the best local dependence model, in general leading to reduced uncertainty when compared to single-station analyses. However, we note that specifying spatial models does require additional assumptions on the dependence structure of the rainfall field. Since our analysis here is primarily diagnostic, we prefer to not introduce additional complexity to the model, and instead use the spatial distribution of the results for understanding the spatially varying effects of the NASH ridge.

6. Conclusions

Our analysis supports the usage of the NASH western ridge position as a relevant predictor in stochastic simulations of rainfall fields, in downscaling climate model simulations, and in risk analyses involving both "wet" and "dry" rainfall extremes. After testing different model dependence structures, we recommend selecting a best model (e.g., using lpml) separately for rainfall occurrence and intensities, as we have shown that these can have different responses to the ridge position. Overall, we found that latitude-dependent models are to be preferred in most of the Southeast, Upper Midwest, and Pacific Northwest. The longitude dependence model is applicable to large parts of the Midwest, while for most of the western United States a simpler model with no dependence is to be preferred, except in the part of the Pacific Northwest. The statistical approach developed here could be adopted with minor modifications to investigate the regional impacts of other climate features, and to account for the interplay of different precipitation mechanisms (Marra et al. 2019; Miniussi et al. 2020b). For example, relevant physical information that could be captured include the occurrence of atmospheric river events over the western United States and western Europe (Lavers and Villarini 2015), or the frequency of cold air intrusion events associated with heavy orographic rainfall (Eghdami and Barros 2019). Another future research direction motivated by the present work is the extension of this statistical framework to precipitation at shorter aggregation time scales, which is further complicated by the lack of long instrumental records, and by the need of accurately capturing the time correlation structure of the precipitation process (Marra et al. 2020).

Acknowledgments. The authors thank Dr. Marco Marani for the useful comments on the first draft of this manuscript. E. Zorzetto prepared this manuscript under Award 80NSSC17K0364 from the National Aeronautics and Space Administration, and under award NA18OAR4320123 from the National Oceanic and Atmospheric Administration, U.S. Department of Commerce. The statements, findings, conclusions, and recommendations are those of the author(s) and do not necessarily reflect the views of the National Oceanic and Atmospheric Administration, or the U.S. Department of Commerce. L. Li acknowledges support from the National Science Foundation (NSF) under Grant ICER-1663138.

Data availability statement. The NOAA GHCN precipitation data are freely available online. The codes used in the analysis, as well as a toolkit for computing rainfall statistics for any gauged site over the CONUS are available on Github (https://github.com/EnricoZorzetto/nash_2020).

APPENDIX A

Dependence Models

Here we formulate the four dependence models on the ridge position introduced in section 3b. The dependence on (x_{nj}, y_{nj}) of a generic real model parameter $\alpha_j \in \mathbb{R}$ (describing, e.g., daily rainfall frequency or intensity in year j) is represented through one of the following four relations:

$$\alpha_j^{(\mathrm{NOD})} = \psi(\alpha_0) \quad \forall \quad j = 1, \ldots, J, \tag{A1}$$

$$\alpha_j^{(\mathrm{LOND})} = \psi(\alpha_0 + \alpha_x x_{nj}) = F_x(x_{nj}|\alpha_0, \alpha_x), \tag{A2}$$

$$\alpha_j^{(\mathrm{LATD})} = \psi(\alpha_0 + \alpha_y y_{nj}) = F_y(y_{nj}|\alpha_0, \alpha_y), \tag{A3}$$

$$\alpha_j^{(\mathrm{LWLD})} = \psi\left[\alpha_0 + \alpha_y y_{nj} \frac{1}{1 + \exp(-\alpha_x x_{nj})}\right] = F_{xy}(x_{nj}, y_{nj}|\alpha_0, \alpha_y, \alpha_x), \tag{A4}$$

with α_0, α_y, α_x real parameters encoding the dependence of α_j on the ridge position (x_{nj}, y_{nj}). The functions F_x, F_y, and F_{xy} here simply express whether there is a dependence on x_{nj}, y_{nj} or both. Equation (A1) represents the case of No Dependence (NOD model), i.e., of a constant parameter α_0 in each year. Equations (A2) and (A3) represent the case of a parameter depending only on the ridge longitudinal or latitudinal position, respectively, while in Eq. (A4) the y_{nj} dependence is modulated by sigmoid function of the normalized ridge longitude x_{nj}. In all four cases, $\psi(\cdot)$ is a generic link function that can be used to generalize the model outlined in Eqs. (A1)–(A4) to the possible case of nonlinear dependence on the ridge position, or to the case of a parameter α_j with support different than the real line $\mathbb{R}$. In Eq. (A4), the exponential term produces a sigmoid function which, varying between 0 and 1, determines the strength of the longitudinal dependence term $\alpha_y x_{nj}$. For example, in the case of negative α_x, the dependence on y_{nj} is more relevant when the ridge is located westward of its mean longitudinal position, while it approaches zero as the ridge moves eastward. The opposite occurs when $\alpha_x > 0$, and in both cases the absolute value $|\alpha_x|$ determines the scale of this effect. We specify a normal prior distribution for α_x, with unit variance and centered around zero [$\alpha_x \sim N(0, 1)$]. Analogously, we choose a similar prior distribution for the parameter [$\alpha_y \sim N(0, 1)$] controlling the y_{nj} dependence. These prior distributions are symmetric around zero, so that all information on the sign of the dependence is directly obtained from rainfall observations.

APPENDIX B

Models for the Seasonal Number of Events

The simplest model considered here is a binomial distribution for n_j. For a season of N_t days (e.g., $N_t = 92$ for our case JJA), the probability mass function of observing n_j events thus reads

$$p(n_j|\pi_{nj}) = \mathrm{Bin}(n_j|\pi_{nj}, N_t) = \binom{N_t}{n_j} \pi_{nj}^{n_j} (1 - \pi_{nj})^{N_t - n_j}. \tag{B1}$$

Different models can be obtained based on the choice of the parameters $\pi_{nj} \in (0, 1)$. In the simplest model with no NASH ridge dependence (NOD), $\pi_{nj} = \pi_n \quad \forall \quad j = 1, .., J$ is the only parameter describing the distribution of the n_j. To include the possible effects of the longitudinal and latitudinal positions of the NASH ridge on the distribution of n_j, we adopt the LWLD model specification for π_{nj}

$$\pi_{nj} = \psi(\eta_{nj}) = \frac{1}{1 + \exp(-\eta_{nj})}, \tag{B2}$$

$$\eta_{nj} = \eta_{n0} + \eta_{ny} y_{nj} \frac{1}{1 + \exp(-\eta_{nx} x_{nj})}. \tag{B3}$$

Finally, we have the case of y_{nj} dependence only (LATD) with $\eta_{nj} = \eta_{n0} + \eta_{ny} y_{nj}$, and the case of x_{nj} dependence (LOND) with $\eta_{nj} = \eta_{n0} + \eta_{nx} x_{nj}$. In the LWLD, LOND, and LATD cases, the link function ψ defined in Eq. (B2) introduces a nonlinear dependence of the distribution of the seasonal number of events on the ridge position, so that the rate of rainfall occurrence π_{nj} is defined in the interval (0, 1). Equation (B3) includes the dependence on the latitude of the ridge position through the linear predictor $\eta_{ny} y_{nj}$, but this dependence is further modulated by the longitude of the ridge through the function of x_{nj}, which, as discussed earlier, can reduce or completely eliminate the model dependence on the latitude y_{nj} based on the longitudinal position of the NASH ridge. The parameters of the LWLD are therefore η_{n0}, η_{ny}, and η_{nx}, to which we assign weakly informative Gaussian prior distributions.

The second model considered for n_j is a Markov chain with transition probabilities between daily wet and dry states are defined as

$$p_{ik} = P(J_t = k|J_{t-1} = i), \tag{B4}$$

where J_t is the binary state at time t, which can have value 0 (dry) or 1 (wet); p_{ik} is the transition probability from state i to state k, with $i, k = 0, 1$. Note that this simple MC (without NASH ridge dependence, NOD) model is completely described by two parameters. We take these to be the wet fraction $\pi^{(\mathrm{MC})} = p_{01}/\beta^{(\mathrm{MC})}$ and the 1-day lag serial correlation $\beta^{(\mathrm{MC})} = p_{11} - p_{01}$. Note that also in the case of this MC model we can construct models of increasing complexity which account for the position of the NASH ridge. As noted in Katz et al. (2003), this conditioning yields an overall model structure unconditional from the NASH ridge position which is more complex than the simple MC. In this case we can again define a LOND, LATD, and LWLD versions of the MC model by first transforming the parameters from (0, 1) to the real line $\mathbb{R}$ through the functions $\pi_j^{(\mathrm{MC})} = 1/[1 + \exp(-\eta_j^{(\mathrm{MC})})]$ and $\beta_j^{(\mathrm{MC})} = 1/[1 + \exp(-\rho_j^{(\mathrm{MC})})]$ for year j. Note that here for simplicity we limit our analysis to the physically relevant case $\beta_j^{(\mathrm{MC})} \in (0, 1)$, thus excluding the possibility of anticorrelated wet–dry sequences at the daily time scale. The four dependence models for the parameters $\eta_j^{(\mathrm{MC})}$ and $\rho_j^{(\mathrm{MC})}$ are summarized in Table B1, with F_x, F_y, and F_{xy} as defined in Eqs. (A2)–(A4), respectively.

APPENDIX C

Model for the Daily Event Rainfall Magnitudes

We model the magnitudes of daily rainfall accumulations h_{ij} in excess of $q = 1\,\mathrm{mm\ day^{-1}}$ in year j with a two-parameter Weibull distribution with probability distribution

TABLE B1. Dependence models for the parameters of the Markov chain described in appendix B.

Model	Rainfall rate parameter	Correlation parameter
NOD	$\eta_j^{(\mathrm{MC})}$	$\rho_j^{(\mathrm{MC})}$
LOND	$\eta_j^{(\mathrm{MC})} = F_x(x_{nj}\|\eta_0^{(\mathrm{MC})}, \eta_x^{(\mathrm{MC})})$	$\rho_j^{(\mathrm{MC})} = F_x(x_{nj}\|\rho_0^{(\mathrm{MC})}, \rho_x^{(\mathrm{MC})})$
LATD	$\eta_j^{(\mathrm{MC})} = F_y(y_{nj}\|\eta_0^{(\mathrm{MC})}, \eta_y^{(\mathrm{MC})})$	$\rho_j^{(\mathrm{MC})} = F_y(y_{nj}\|\rho_0^{(\mathrm{MC})}, \rho_y^{(\mathrm{MC})})$
LWLD	$\eta_j^{(\mathrm{MC})} = F_{xy}(x_{nj}, y_{nj}\|\eta_0^{(\mathrm{MC})}, \eta_y^{(\mathrm{MC})}, \eta_x^{(\mathrm{MC})})$	$\rho_j^{(\mathrm{MC})} = F_{xy}(x_{nj}, y_{nj}\|\rho_0^{(\mathrm{MC})}, \rho_y^{(\mathrm{MC})}, \rho_x^{(\mathrm{MC})})$

$$f_w(h;\gamma_j,\delta_j) = \frac{\gamma_j}{\delta_j}\left(\frac{h}{\delta_j}\right)^{(\gamma_j-1)} \exp\left[-\left(\frac{h}{\delta_j}\right)^{\gamma_j}\right], \qquad \text{(C1)}$$

with scale and shape parameters $\delta_j \in \mathbb{R}^+$ and $\gamma_j \in \mathbb{R}^+$, respectively. For all dependence models, we do not allow the Weibull shape parameter to vary ($\gamma_j = \gamma \quad \forall \quad j = 1, \ldots, J$), thus assuming that the position of the NASH ridge primarily affects the characteristic intensity of the daily events, which is encoded in the seasonal Weibull scale parameters δ_j. For the scale parameter we have $\delta_j = \delta \quad \forall \quad j = 1, \ldots, J$ (NOD model), $\log(\delta_j) = F_x(x_{nj}|\delta_0, \delta_x)$ (LOND model), $\log(\delta_j) = F_y(y_{nj}|\delta_0, \delta_y)$ (LATD model), and $\log(\delta_j) = F_{xy}(x_{nj}, y_{nj}|\delta_0, \delta_y, \delta_x)$ (LWLD model).

APPENDIX D

Model for the Seasonal Total Rainfall Accumulations

We model seasonal total rainfall amounts using a Weibull distribution (Laherrère and Sornette 1998; Sornette 2006) with pdf defined in Eq. (C1). We include an atom of probability in zero corresponding to the case of a completely dry season, modeled through a binomial random variable with a small prior probability of observing a completely dry summer. The distribution of the seasonal rainfall total in year j is thus described by the Weibull shape and scale parameters $\gamma^{(s)} \in \mathbb{R}^+$ and $\delta_j^{(s)} \in \mathbb{R}^+$, and by a binomial rate parameter $\pi^{(s)} \in (0, 1)$ representing the probability of a completely dry summer. Here we assume that the parameters $\pi^{(s)}$ and $\gamma^{(s)}$ do not depend on the NASH ridge positions, and we choose a weakly informative prior for $\gamma^{(s)}$. For $\pi^{(s)}$ we select a prior distribution with most of the mass close to zero (as ordinarily we do not expect many completely dry summers). For the scale parameter, we introduce the four dependence models introduced in Eqs. (A1)–(A4). First, the NOD model with no dependence on the ridge position ($\delta_j^{(s)} = \delta^{(s)} \quad \forall j = 1, .., J$). Second, the LOND model where $\delta_j^{(s)}$ only depends on the ridge longitude: $\log(\delta_j^{(s)}) = F_x(x_{nj}|\delta_0^{(s)}, \delta_x^{(s)})$. Third, LATD with $\log(\delta_j^{(s)}) = F_y(y_{nj}|\delta_0^{(s)}, \delta_y^{(s)})$. Last, the LWLD model with $\log(\delta_j^{(s)}) = F_{xy}(x_{nj}, y_{nj}|\delta_0^{(s)}, \delta_y^{(s)}, \delta_x^{(s)})$.

APPENDIX E

Evaluation of Predictive Accuracy

Following Gelman et al. (2013), the log posterior predictive density (lppd) for a sample of observations y_j, $j = 1, \ldots, M$ (where y_j could be, e.g., daily rainfall occurrences n_j or intensities h_{ij}) given a statistical model $p(y_i|\theta^{(s)})$ with parameters $\theta^{(s)}$ can be computed from S MCMC draws as

$$\mathrm{lppd} = \sum_{i=1}^{M} \log\left[\frac{1}{S}\sum_{s=1}^{S} p(y_i|\theta^{(s)})\right]. \qquad \text{(E1)}$$

However, this quantity overestimates the predictive performance of a model as it does not assess a model's tendency to overfit the sample used for calibration. To correct for this here we use the logarithm of the pseudomarginal likelihood (lpml) (Gelfand and Dey 1994):

$$\mathrm{lpml} = \sum_{i=1}^{M} \log(\mathrm{CPO}_i), \qquad \text{(E2)}$$

where CPO_i is the conditional predictive ordinate (Gelfand et al. 1992; Gelfand and Dey 1994), which estimates the leave-one-out probability of observing a value y_i given that y_{-i} has been observed. CPO_i can be computed as the geometric mean of the likelihood of the data given the model. From S MCMC samples,

$$\mathrm{CPO}_i \simeq \left[\frac{1}{S}\sum_{s=1}^{S}\frac{1}{p(y_i|\theta^{(s)})}\right]^{-1}. \qquad \text{(E3)}$$

When comparing the four difference types of dependence on the NASH ridge position considered here [Eqs. (A1)–(A4)], the model with the largest value of lpml is considered the best model for a given station record. Note that using the lppd [Eq. (E1)] would consistently select the most complex model (i.e., the model with dependence on both x_{nj} and y_{nj}, or the model with longitudinal dependence only). For a comparison of the results obtained using lppd and lpml for each variable considered here, we refer the reader to the online supplemental material.

APPENDIX F

List of Acronyms

NASH	North Atlantic subtropical high
CONUS	Conterminous United States
BHI	Bermuda high index
USHCN	U.S. Historical Climatology Network
JJA	June–August (months)
NOD	No Dependence (model)
LOND	Longitudinal Dependence (model)
LATD	Latitudinal Dependence (model)
LWLD	Longitude-Weighted Latitudinal Dependence (model)
MC	Markov chain

MCMC	Markov chain Monte Carlo
lppd	Log posterior predictive density
lpml	Log posterior marginal likelihood
CPO	Conditional predictive ordinate

REFERENCES

Allan, R. P., and B. J. Soden, 2008: Atmospheric warming and the amplification of precipitation extremes. *Science*, **321**, 1481–1484, https://doi.org/10.1126/science.1160787.

Bishop, D. A., A. P. Williams, and R. Seager, 2019a: Increased fall precipitation in the southeastern United States driven by higher-intensity, frontal precipitation. *Geophys. Res. Lett.*, **46**, 8300–8309, https://doi.org/10.1029/2019GL083177.

——, and Coauthors, 2019b: Investigating the causes of increased twentieth-century fall precipitation over the southeastern United States. *J. Climate*, **32**, 575–590, https://doi.org/10.1175/JCLI-D-18-0244.1.

Carpenter, B., and Coauthors, 2017: Stan: A probabilistic programming language. *J. Stat. Software*, **76**, https://doi.org/10.18637/jss.v076.i01.

Diem, J. E., 2006: Synoptic-scale controls of summer precipitation in the southeastern United States. *J. Climate*, **19**, 613–621, https://doi.org/10.1175/JCLI3645.1.

——, 2013: Influences of the Bermuda high and atmospheric moistening on changes in summer rainfall in the Atlanta, Georgia region, USA. *Int. J. Climatol.*, **33**, 160–172, https://doi.org/10.1002/joc.3421.

Eghdami, M., and A. P. Barros, 2019: Extreme orographic rainfall in the eastern Andes tied to cold air intrusions. *Front. Environ. Sci.*, **7**, 101, https://doi.org/10.3389/fenvs.2019.00101.

Gamble, D. W., D. B. Parnell, and S. Curtis, 2008: Spatial variability of the Caribbean mid-summer drought and relation to north Atlantic high circulation. *Int. J. Climatol.*, **28**, 343–350, https://doi.org/10.1002/joc.1600.

Gelfand, A. E., and D. K. Dey, 1994: Bayesian model choice: Asymptotics and exact calculations. *J. Roy. Stat. Soc.*, **56B**, 501–514, https://doi.org/10.1111/j.2517-6161.1994.tb01996.x.

——, ——, and H. Chang, 1992: Model determination using predictive distributions with implementation via sampling-based methods. Tech. Rep. 462, Office of Naval Research, 38 pp., https://apps.dtic.mil/dtic/tr/fulltext/u2/a258777.pdf.

Gelman, A., J. B. Carlin, H. S. Stern, D. B. Dunson, A. Vehtari, and D. B. Rubin, 2013: *Bayesian Data Analysis*. Chapman and Hall/CRC, 675 pp.

Hoskins, B. J., 1991: Towards a pv-θ view of the general circulation. *Tellus*, **43A**, 27–36, https://doi.org/10.3402/tellusa.v43i4.11936.

Hosseini, S., M. Scaioni, and M. Marani, 2020: Extreme Atlantic hurricane probability of occurrence through the metastatistical extreme value distribution. *Geophys. Res. Lett.*, **47**, 2019GL086138, https://doi.org/10.1029/2019GL086138.

Hu, Q., S. Feng, and R. J. Oglesby, 2011: Variations in north American summer precipitation driven by the Atlantic multidecadal oscillation. *J. Climate*, **24**, 5555–5570, https://doi.org/10.1175/2011JCLI4060.1.

Kalnay, E., and Coauthors, 1996: The NCEP/NCAR 40-Year Reanalysis Project. *Bull. Amer. Meteor. Soc.*, **77**, 437–472, https://doi.org/10.1175/1520-0477(1996)077<0437:TNYRP>2.0.CO;2.

Kasahara, A., 1959: A comparison between geostrophic and nongeostrophic numerical forecasts of hurricane movement with the barotropic steering model. *J. Meteor.*, **16**, 371–384, https://doi.org/10.1175/1520-0469(1959)016<0371:ACBGAN>2.0.CO;2.

Katz, R. W., and X. Zheng, 1999: Mixture model for overdispersion of precipitation. *J. Climate*, **12**, 2528–2537, https://doi.org/10.1175/1520-0442(1999)012<2528:MMFOOP>2.0.CO;2.

——, M. B. Parlange, and C. Tebaldi, 2003: Stochastic modeling of the effects of large-scale circulation on daily weather in the southeastern U.S. *Issues in the Impacts of Climate Variability and Change on Agriculture*, L. O. Mearns, Ed., Springer, 189–216.

Keim, B. D., 1997: Preliminary analysis of the temporal patterns of heavy rainfall across the southeastern United States. *Prof. Geogr.*, **49**, 94–104, https://doi.org/10.1111/0033-0124.00060.

Kunkel, K. E., and Coauthors, 2013: Monitoring and understanding trends in extreme storms: State of knowledge. *Bull. Amer. Meteor. Soc.*, **94**, 499–514, https://doi.org/10.1175/BAMS-D-11-00262.1.

Laherreère, J., and D. Sornette, 1998: Stretched exponential distributions in nature and economy: "Fat tails" with characteristic scales. *Eur. Phys. J.*, **2B**, 525–539, https://doi.org/10.1007/s100510050276.

Lavers, D. A., and G. Villarini, 2015: The contribution of atmospheric rivers to precipitation in Europe and the United States. *J. Hydrol.*, **522**, 382–390, https://doi.org/10.1016/j.jhydrol.2014.12.010.

Li, L., and W. Li, 2013: Southeastern United States summer rainfall framework and its implication for seasonal prediction. *Environ. Res. Lett.*, **8**, 044017, https://doi.org/10.1088/1748-9326/8/4/044017.

——, ——, and Y. Kushnir, 2012: Variation of the North Atlantic subtropical high western ridge and its implication to southeastern us summer precipitation. *Climate Dyn.*, **39**, 1401–1412, https://doi.org/10.1007/s00382-011-1214-y.

Li, W., L. Li, R. Fu, Y. Deng, and H. Wang, 2011: Changes to the North Atlantic subtropical high and its role in the intensification of summer rainfall variability in the southeastern United States. *J. Climate*, **24**, 1499–1506, https://doi.org/10.1175/2010JCLI3829.1.

——, ——, M. Ting, and Y. Liu, 2012: Intensification of northern hemisphere subtropical highs in a warming climate. *Nat. Geosci.*, **5**, 830–834, https://doi.org/10.1038/ngeo1590.

Lins, H. F., and T. A. Cohn, 2011: Stationarity: Wanted dead or alive? *J. Amer. Water Resour. Assoc.*, **47**, 475–480, https://doi.org/10.1111/j.1752-1688.2011.00542.x.

Liu, Y., G. Wu, and R. Ren, 2004: Relationship between the subtropical anticyclone and diabatic heating. *J. Climate*, **17**, 682–698, https://doi.org/10.1175/1520-0442(2004)017<0682:RBTSAA>2.0.CO;2.

Mallakpour, I., and G. Villarini, 2015: The changing nature of flooding across the central United States. *Nat. Climate Change*, **5**, 250–254, https://doi.org/10.1038/nclimate2516.

Marani, M., and M. Ignaccolo, 2015: A metastatistical approach to rainfall extremes. *Adv. Water Resour.*, **79**, 121–126, https://doi.org/10.1016/j.advwatres.2015.03.001.

Marra, F., E. I. Nikolopoulos, E. N. Anagnostou, and E. Morin, 2018: Metastatistical extreme value analysis of hourly rainfall from short records: Estimation of high quantiles and impact of measurement errors. *Adv. Water Resour.*, **117**, 27–39, https://doi.org/10.1016/j.advwatres.2018.05.001.

——, D. Zoccatelli, M. Armon, and E. Morin, 2019: A simplified MEV formulation to model extremes emerging from multiple nonstationary underlying processes. *Adv. Water Resour.*, **127**, 280–290, https://doi.org/10.1016/j.advwatres.2019.04.002.

——, M. Borga, and E. Morin, 2020: A unified framework for extreme subdaily precipitation frequency analyses based on

ordinary events. *Geophys. Res. Lett.*, **47**, e2020GL090209, https://doi.org/10.1029/2020GL090209.

Menne, M. J., I. Durre, R. S. Vose, B. E. Gleason, and T. G. Houston, 2012a: An overview of the Global Historical Climatology Network-Daily database. *J. Atmos. Oceanic Technol.*, **29**, 897–910, https://doi.org/10.1175/JTECH-D-11-00103.1.

——, and Coauthors, 2012b: Global historical climatology network-daily (GHCN-Daily), version 3. NOAA National Climatic Data Center, accessed 24 October 2019, https://doi.org/10.7289/V5D21VHZ.

Milly, P., J. Betancourt, M. Falkenmark, R. M. Hirsch, Z. W. Kundzewicz, D. P. Lettenmaier, and R. J. Stouffer, 2008: Stationarity is dead: Whither water management? *Earth*, **319**, 573–574, https://doi.org/10.1126/science.1151915.

Miniussi, A., M. Marani, and G. Villarini, 2020a: Metastatistical extreme value distribution applied to floods across the continental United States. *Adv. Water Resour.*, **136**, 103498, https://doi.org/10.1016/j.advwatres.2019.103498.

——, G. Villarini, and M. Marani, 2020b: Analyses through the metastatistical extreme value distribution identify contributions of tropical cyclones to rainfall extremes in the eastern United States. *Geophys. Res. Lett.*, **47**, e2020GL087238, https://doi.org/10.1029/2020GL087238.

Miyasaka, T., and H. Nakamura, 2005: Structure and formation mechanisms of the Northern Hemisphere summertime subtropical highs. *J. Climate*, **18**, 5046–5065, https://doi.org/10.1175/JCLI3599.1.

Montanari, A., and D. Koutsoyiannis, 2014: Modeling and mitigating natural hazards: Stationarity is immortal! *Water Resour. Res.*, **50**, 9748–9756, https://doi.org/10.1002/2014WR016092.

Nieto Ferreira, R., and T. M. Rickenbach, 2020: Effects of the North Atlantic subtropical high on summertime precipitation organization in the southeast United States. *Int. J. Climatol.*, **40**, 5987–6001, https://doi.org/10.1002/joc.6561.

Papalexiou, S., D. Koutsoyiannis, and C. Makropoulos, 2013: How extreme is extreme? An assessment of daily rainfall distribution tails. *Hydrol. Earth Syst. Sci.*, **17**, 851–862, https://doi.org/10.5194/hess-17-851-2013.

Papalexiou, S. M., and A. Montanari, 2019: Global and regional increase of precipitation extremes under global warming. *Water Resour. Res.*, **55**, 4901–4914, https://doi.org/10.1029/2018WR024067.

——, A. AghaKouchak, and E. Foufoula-Georgiou, 2018: A diagnostic framework for understanding climatology of tails of hourly precipitation extremes in the United States. *Water Resour. Res.*, **54**, 6725–6738, https://doi.org/10.1029/2018WR022732.

Pendergrass, A. G., R. Knutti, F. Lehner, C. Deser, and B. M. Sanderson, 2017: Precipitation variability increases in a warmer climate. *Sci. Rep.*, **7**, 17966, https://doi.org/10.1038/s41598-017-17966-y.

Ryu, J.-H., and K. Hayhoe, 2014: Understanding the sources of Caribbean precipitation biases in CMIP3 and CMIP5 simulations. *Climate Dyn.*, **42**, 3233–3252, https://doi.org/10.1007/s00382-013-1801-1.

Schiermeier, Q., 2010: The real holes in climate science. *Nature*, **463**, 284–287, https://doi.org/10.1038/463284a.

Serinaldi, F., and C. G. Kilsby, 2015: Stationarity is undead: Uncertainty dominates the distribution of extremes. *Adv. Water Resour.*, **77**, 17–36, https://doi.org/10.1016/j.advwatres.2014.12.013.

Sharma, A., C. Wasko, and D. P. Lettenmaier, 2018: If precipitation extremes are increasing, why aren't floods? *Water Resour. Res.*, **54**, 8545–8551, https://doi.org/10.1029/2018WR023749.

Song, F., L. R. Leung, J. Lu, and L. Dong, 2018: Future changes in seasonality of the North Pacific and North Atlantic subtropical highs. *Geophys. Res. Lett.*, **45**, 11 959–11 968, https://doi.org/10.1029/2018GL079940.

Sornette, D., 2006: *Critical Phenomena in Natural Sciences: Chaos, Fractals, Selforganization and Disorder: Concepts and Tools*. 2nd ed. Springer, 528 pp.

Stechmann, S. N., and J. D. Neelin, 2014: First-passage-time prototypes for precipitation statistics. *J. Atmos. Sci.*, **71**, 3269–3291, https://doi.org/10.1175/JAS-D-13-0268.1.

van der Wiel, K., and Coauthors, 2016: The resolution dependence of contiguous us precipitation extremes in response to CO_2 forcing. *J. Climate*, **29**, 7991–8012, https://doi.org/10.1175/JCLI-D-16-0307.1.

Westra, S., and Coauthors, 2014: Future changes to the intensity and frequency of short-duration extreme rainfall. *Rev. Geophys.*, **52**, 522–555, https://doi.org/10.1002/2014RG000464.

Wilson, P., and R. Toumi, 2005: A fundamental probability distribution for heavy rainfall. *Geophys. Res. Lett.*, **32**, L14812, https://doi.org/10.1029/2005GL022465.

Wu, G., and Y. Liu, 2003: Summertime quadruplet heating pattern in the subtropics and the associated atmospheric circulation. *Geophys. Res. Lett.*, **30**, 1201, https://doi.org/10.1029/2002GL016209.

Zorzetto, E., and M. Marani, 2019: Downscaling of rainfall extremes from satellite observations. *Water Resour. Res.*, **55**, 156–174, https://doi.org/10.1029/2018WR022950.

——, and ——, 2020: Extreme value metastatistical analysis of remotely sensed rainfall in ungauged areas: Spatial downscaling and error modelling. *Adv. Water Resour.*, **135**, 103483, https://doi.org/10.1016/j.advwatres.2019.103483.

——, G. Botter, and M. Marani, 2016: On the emergence of rainfall extremes from ordinary events. *Geophys. Res. Lett.*, **43**, 8076–8082, https://doi.org/10.1002/2016GL069445.